# Dynamic data acquisition for optical coherence tomography system

**Dual Degree Project Stage 1 Report**


SUBMITTED BY

**Thunguri Prathyush Kumar**
**Roll No : 190100129**

SUPERVISOR

**Prof. Sripriya Ramamoorthy**

*Department of Mechanical Engineering*

**INDIAN INSTITUTE OF TECHNOLOGY**

**BOMBAY - 400 076 (INDIA)**


**October - 2023**

# Contents

# List of Figures

# List of Tables

# Chapter 1

# Introduction

Historically, medical practitioners and researchers have relied on various imaging techniques to gain insights into the human body's inner workings. These techniques ranged from X-rays to ultrasound and magnetic resonance imaging (MRI). However, these conventional imaging techniques possessed inherent limitations, often restricting their ability to provide high-resolution, real-time, and minimally invasive imaging of *in vivo* tissue structures.

X-rays, for instance, offered excellent penetration but could not differentiate soft tissues effectively. Ultrasound provided real-time imaging but struggled with limited resolution and depth penetration. While offering exceptional soft tissue contrast, MRI was slow and expensive, limiting its utility for many clinical applications.Another imaging technique, Low-Coherence Interferometry (LCI), also emerged on the scene, offering high-resolution imaging capabilities. However, LCI, like its predecessors, had its limitations, including challenges with real-time imaging, a lack of cross-sectional imaging, and its applicability to specific clinical scenarios.

These limitations prompted researchers to explore alternatives that could bridge the gaps left by existing imaging technologies. As we will discover in this report, Optical Coherence Tomography (OCT) emerged as a groundbreaking solution to these challenges, offering high-resolution, real-time, non-invasive imaging capabilities that revolutionized our understanding of biological tissues.

Tomlins and Wang [5] have conducted an in-depth examination of the progress, operational principles, and wide-ranging applications of OCT. In their comprehensive review, they provide a foundational introduction to the theory behind OCT and explore various modalities in which this imaging technique can be applied. These modalities encompass time-domain, frequency-domain, Doppler, and quantum-domain approaches. Furthermore, Tomlins and Wang [5] offer valuable insights by presenting an overview of the comparative sensitivity levels between time and frequency domain modalities, shedding light on the strengths and limitations of each in OCT applications.

OCT has widespread applications, revolutionizing ophthalmology by diagnosing eye conditions like glaucoma and macular degeneration. In dermatology, it aids in skin disorder diagnosis and wound assessment. Cardiologists use Intravascular OCT (IV-OCT) for coronary artery imaging. Otolaryngologists visualize the middle ear and throat, while gastroenterologists inspect the gastrointestinal tract with OCT. Dentists use it for oral health assessments.

## 1.1 Aim

## 1.2 Organization of the report

The organization of the report is as follows: *Chapter 2* delves into the foundational theory of Optical Coherence Tomography (OCT), encompassing both hardware and software components employed in our research. In *Chapter 3*, a concise literature review contextualizes our project within the broader scientific landscape. *Chapter 4* provides a comprehensive account of the research conducted thus far, detailing the milestones achieved during this study. Lastly, *Chapter 5* outlines the second phase of our work, shedding light on the anticipated outcomes and implications of Stage 2 of the research project.

# Chapter 2

# Theory

Optical Coherence Tomography (OCT) is a non-invasive medical imaging technology used for visualizing the internal structures of various biological tissues, particularly in ophthalmology and cardiology. OCT employs interferometry principles and low-coherence light to create high-resolution, cross-sectional images of biological tissues.

## 2.1 OCT system

The OCT system employs a Michelson interferometer for the interferometry process. The Michelson interferometer is primarily utilized to measure the interference of light waves, yielding valuable insights into the properties of light, objects, and the surrounding environment. A Michelson interferometer starts with a beam splitter, typically a partially reflecting glass or optical component. It divides an incoming light beam into two distinct beams: one that is transmitted through the beam splitter and another that is reflected by it. The transmitted beam, often called the ”reference beam,” is directed toward a stationary mirror known as the reference mirror. This mirror reflects the reference beam towards the beam splitter. The other beam, termed the ”sample beam,” is directed toward a sample or measuring mirror. The positioning of this mirror can be adjusted to vary the path length of the sample beam. Subsequently, these two beams—the reference beam and the sample beam—are recombined at the beam splitter. This recombination results in the interference of the two beams, giving rise to an interference pattern.

In the context of OCT, a broadband optical field is employed, facilitating the possibility of interference between optical fields only when the reference and optical path lengths align closely within the coherence length. This coherence length represents the distance over which light waves maintain their synchronized phase relationship. For meaningful interference to happen in OCT, the lengths of the reference and sample arms need to be in sync within the range defined by the coherence length of the light source being used. Distinct variations in the refractive index between layers within the sample medium are evident through corresponding intensity peaks observed in the interference pattern.

We use Low coherence light for the OCT due to its ability to provide precise depth information. It generates light with a very narrow bandwidth, resulting in a short coherence length. This means that when light interacts with the target, it primarily interferes with waves from the same depth. This characteristic allows OCT to discern structures at

different depths accurately, ensuring sharp, clear imaging of tissue layers and structures without unwanted blurring or interference from adjacent layers.

The intensity pattern obtained to obtain optical structure of sample can be measured using both time and frequency domains, both of these techniques are discussed in the following section.

### 2.1.1 Time Domain OCT

In Time-Domain OCT (TD-OCT), when imaging a multi-layered sample with various depths, each layer creates different optical path lengths. To obtain intensity peaks and depth information for each layer, the reference mirror is continuously translated so that it remains within one coherence length of the light source. This continuous translation of the reference mirror allows the TD-OCT system to capture the interference signal at various depths within the sample. By scanning the sample with the continuous motion of the reference mirror, a series of depth profiles are generated, revealing the structural details of the multi-layered sample.

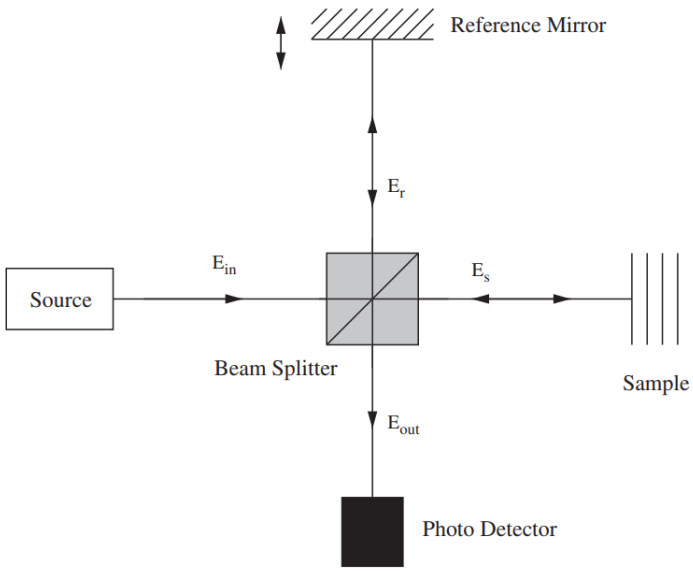


Figure 2.1: Time Domain OCT system [5]

Figure 2.1 shows the schematic of the Time Domain OCT system described above the double edged arrow indicating the reference mirror can be translated to obtain depth information of each layer in the sample.

### 2.1.2 Frequency Domain OCT

Frequency Domain OCT (FD-OCT) extends the working principles of TD-OCT by introducing a more efficient data acquisition approach. In FD-OCT, instead of the continuous movement of the reference mirror over time, mirror is kept stationary and it employs a spectrometer to simultaneously measure the interference spectrum of reflected light at various wavelengths.

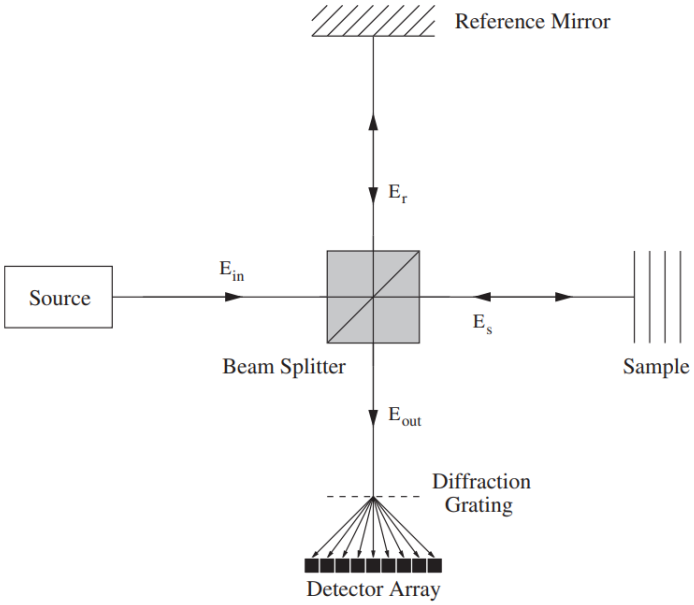


Figure 2.2: Frequency Domain OCT system [5]

The interference spectrum measured by the spectrometer contains information about the depths of various structures within the sample but in the form of wavelengths. By performing a Fourier transformation on the interference spectrum data, FD-OCT can convert these wavelength-based measurements into spatial information. This transformation maps the optical path differences to corresponding depth locations within the sample. Unlike TD-OCT, FD-OCT takes only a single scan, namely an A-scan, to get the entire depth information of the multi-layered sample. FD-OCT is also known as Spectral Domain OCT (SD-OCT).

## 2.2 Telesto - III

The SD-OCT system we are using in the laboratory for the experiment and data acquisition is Telesto - III (TEL320) manufactured by a American company Thorlabs, Inc. The specifications of the system is as follows.

| | |
|---|---|
| Central wavelength | 1310 nm |
| Bandwidth | 150 ($\pm$ 75mm) |
| Axial scan rate | 10 kHz to 146 kHz |
| Maximum imaging depth (in air) | 3.56 mm |
| Maximum aerial field of view | 1cm x 1cm |
| Axial resolution (in air) | 3.48 $\mu$m |
| Lateral resolution at focus with OCT scan lens kit | 13 $\mu$m |

Table 2.1: Specifications of TELESTO - III [3]

The Telesto III system is operated through specialized software known as ThorImage. Additional details regarding its functionality and usage will be provided in the subsequent section.

## 2.3 ThorImage

In this research, the OCT system is seamlessly integrated with the powerful data acquisition software ThorImageOCT. This sophisticated 64-bit Windows-based software plays a pivotal role in our experimental setup, facilitating the acquisition and visualization of OCT data. Notably, it offers interactive scan position control via video display, catering to standard line and freeform pattern scans. Moreover, ThorImageOCT boasts advanced dataset management capabilities, providing access to raw spectra, processed data, and all essential calibration files for custom-designed processing routines.

In addition to its data handling capabilities, this software offers high-speed volume rendering of three-dimensional data, enhancing our ability to visualize complex structures. Furthermore, it supports advanced imaging techniques such as Doppler and speckle variance imaging, enabling us to explore dynamic tissue characteristics. The software also provides versatile control over scanning and acquisition parameters, including options for averaging and adjustable scan speeds.

ThorImageOCT, as an integral part of our research framework, empowers us to collect and analyze OCT data efficiently, contributing to the comprehensive investigation and understanding of our experimental objectives.

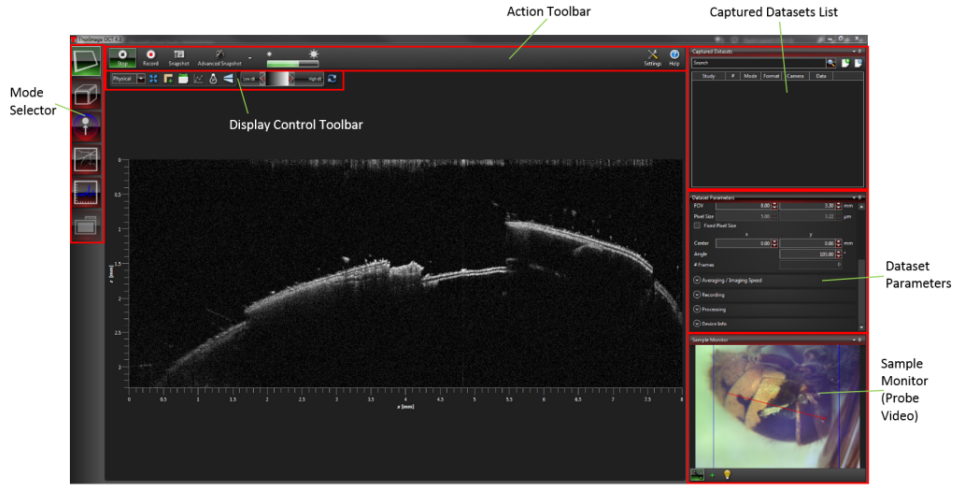


Figure 2.3: ThorImage software [4]

Nonetheless, it's important to acknowledge certain limitations associated with the ThorImage software. A notable constraint is the presence of a barrier that restricts us to acquire a maximum of 10,000 continuous A-scans within a B-scan. This limitation poses challenges, particularly when aiming to reduce noise in our data, as achieving greater precision often necessitates a larger number of A-scans. To address this issue, Thorlabs offers an alternative solution: a C++ software development kit (SDK) furnished with base code that encompasses a majority of the essential functions (to be discussed in forthcoming chapters). Consequently, our strategy involves customizing and adapting the SDK to cater to our specific research requirements, allowing us to overcome these limitations and extract more valuable insights from our OCT data.

# Chapter 3

# Literature Review

## 3.1 Lin et al (2018) [2]

This paper outlines the adaptation of the Thorlabs Telesto, a commercially available Spectral Domain Optical Coherence Tomography (SDOCT) system, for precise displacement measurements within the cochlea using Spectral Domain Phase Microscopy (SDPM). The paper thoroughly discusses the essential software and hardware modifications required to integrate the Telesto with a Tucker-Davis Technologies data acquisition system, enabling the acquisition of synchronized vibration and electrophysiological data from the gerbil cochlea. By making this advanced imaging system accessible, it empowers a broader community of auditory researchers to leverage its capabilities for auditory displacement measurements.

The processing steps shown in the paper are explained below.

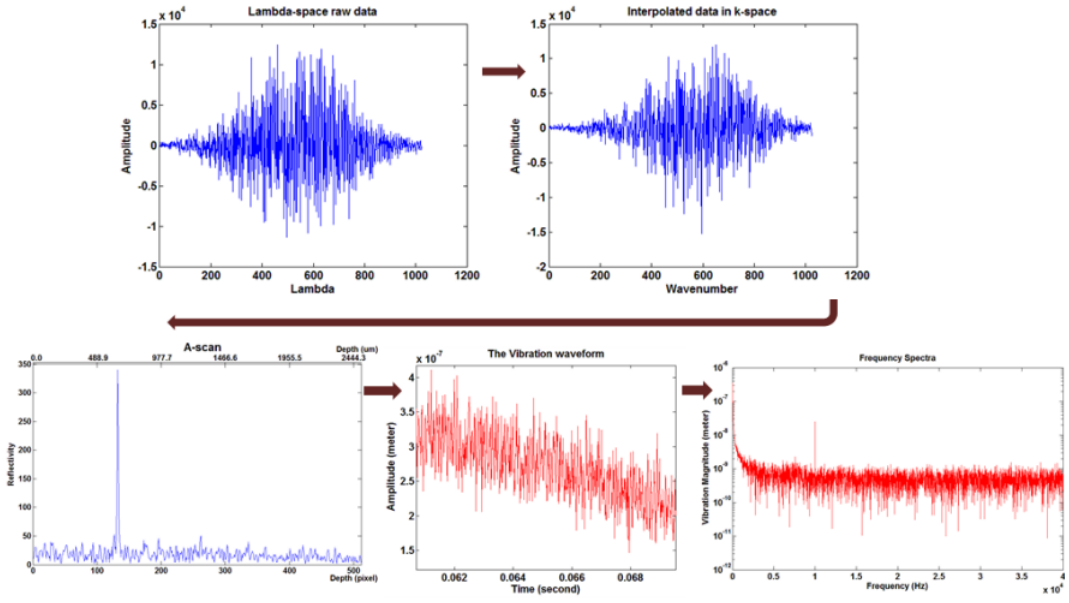


Figure 3.1: The flow diagram of the SDOCT data processing steps [1]

Figure 3.1 outlines the essential steps in processing SD-OCT data to extract motion information from spectrometer data. Initially, when the sample and reference beams interfere, they form an interferogram, which is subsequently directed to a spectrometer where the beam is separated into its constituent wavelengths. This data undergoes a series of processing steps to extract vibration-related information.

The process commences with the interpolation of interferogram data, transitioning it from the wavelength domain to the wavenumber domain. Subsequently, an inverse Fourier transform is applied to this transformed data, yielding complex A-scan data. The magnitude of this complex A-scan indicates the depth profile of the sample. Meanwhile, observing the phase variation of the A-scan over time reveals the vibration waveform. Further analysis, through Fourier transform, of this vibration waveform shows the motion, including amplitude, phase, and frequency characteristics.

## Matlab data processing

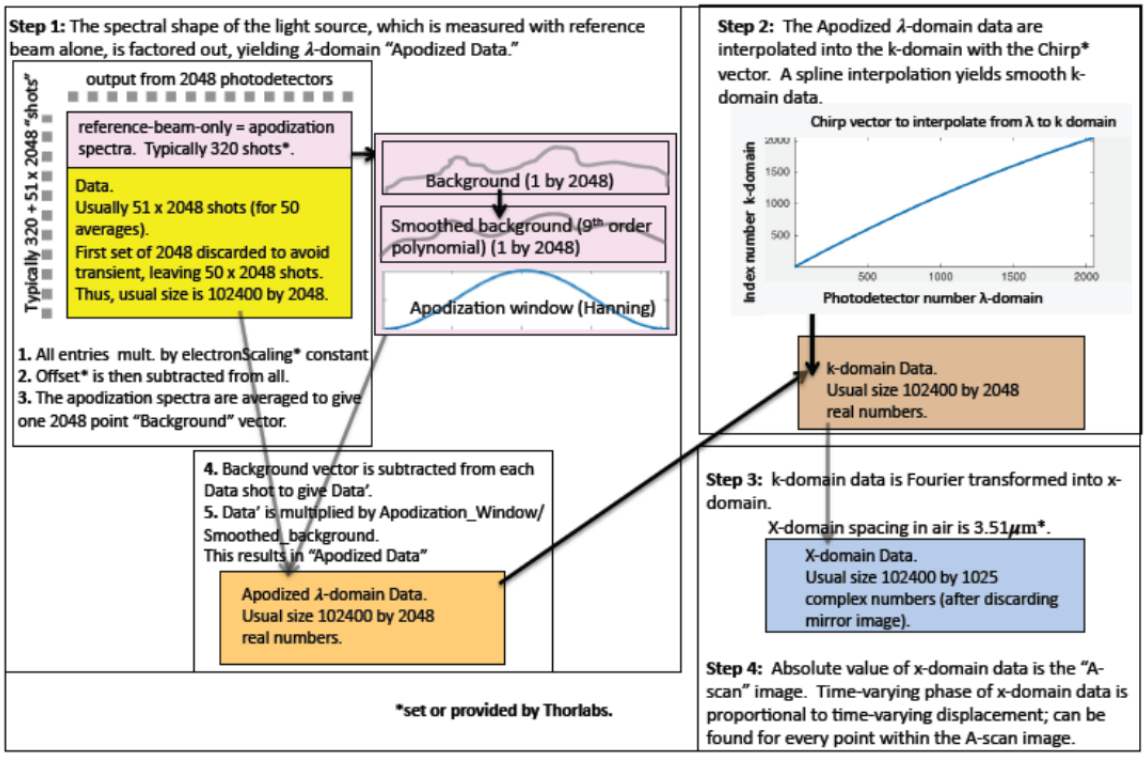


Figure 3.2: The flow chart of the processing steps of the SDOCT spectrometer data [1]

The Figure 3.2 shows a flow chart of the processing steps of the SDOCT spectrometer data. In step 1, the spectrometer data is reference subtracted, windowed, and apodized. Then, the data is interpolated to the k-domain in step 2 with a chirp vector. Step 3, the complex A-scan is generated through the Fourier transform of the linearly-spaced k-domain data.

## 3.2 Wang and Nuttall (2010) [6]

Wang and Nuttall presents a novel method for imaging the motion of cellular compartments within the organ of Corti in guinea pigs at a subnanometer scale. The method, called phase-sensitive optical coherence tomography (PSOCT), is based on the measurement of the phase changes of spectral interferograms induced by localized tissue motion. Analysis of the spectral interferograms showed that conventional spectral domain OCT is capable of providing sufficient sensitivity to measure depth-resolved vibrations.

The organ of Corti is the sensory organ of the inner ear that is responsible for hearing. It is a complex structure that contains a variety of different cell types, including outer hair cells (OHCs). OHCs play a critical role in hearing by amplifying sound signals. However, the biomechanical mechanisms of how OHCs work are not fully understood.

# Chapter 4

# Current Work

## 4.1 Frequency Sweep

A frequency sweep, also referred to as frequency scanning or frequency modulation, is a deliberate variation of frequency over time. It entails the systematic alteration of a signal's frequency within a specified range, either continuously or in discrete steps. In our research experiment, we incorporate vibrometry measurements alongside OCT. This necessitates the use of a frequency sweep signal as input to a speaker. Currently, our setup lacks a dedicated Digital-to-Analog Converter (DAC) port to directly provide the sound signal. To circumvent this limitation, we are utilizing an external device to trigger a separate signal generator, which operates independently of the ThorImage software. Our objective is to develop code that seamlessly integrates with the C++ SDK and facilitates vibrometry experiments without the need for external interventions, streamlining the data acquisition process and enhancing the overall efficiency of our experiment.

### MATLAB code for tone burst signal shown in Figure 4.1

```
clear all;
close all;
clc;
% Parameters
frequency = 1; % Frequency of the wave (in Hz)
maxAmplitude = 5; % Maximum amplitude of the wave
duration = 10; % Duration of the wave (in seconds)
samplingRate = 44100; % Sampling rate (in Hz)
maxDuration = 7; % Duration of pause at max amplitude (in seconds)
% Time vector
t = linspace(0, duration, duration * samplingRate);
% Generate the wave
maxSamples = round(maxDuration * samplingRate); % No.of samples in maxduration
amplitude = [linspace(0, maxAmplitude, numel(t)/2-maxSamples/2),
    maxAmplitude*ones(1, maxSamples), linspace(maxAmplitude,0,
```

```
    numel(t)/2-maxSamples/2)];
wave = amplitude .* sin(2*pi*frequency*t);
% Plot the wave
plot(t, wave)
xlabel('Time (s)')
ylabel('Amplitude')
title('Tone burst signal at single frequency')
```

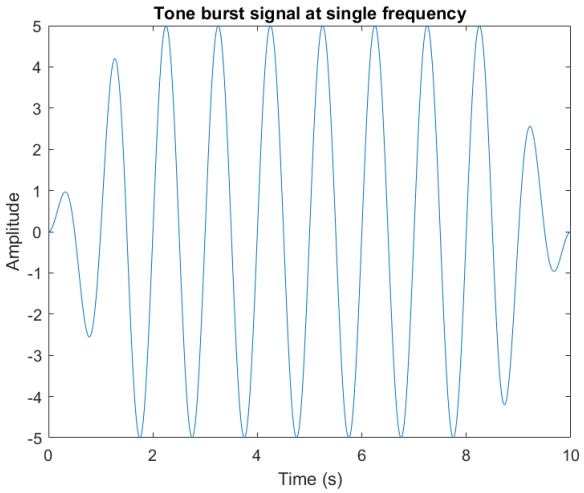


Figure 4.1: Tone burst signal for single frequency in time domain

### MATLAB code for frequency sweep signal shown in Figure 4.2

```
clear all;
close all;
clc;
% Parameters
frequencyA = 1; % Starting frequency
frequencyB = 5; % Ending frequency
numFrequencies = 10; % Number of frequencies
maxAmplitude = 5; % Maximum amplitude of the wave
Totduration = 10; % Total duration of the wave (in sec)
dutycycle = 0.8; % duty cycle for single frequency
samplingRate = 44100; % Sampling rate (in Hz)
maxDuration = 7; % Duration of pause at max amplitude (in sec)
%duty cycle allotment
duration = dutycycle*Totduration; % duration of wave (in sec)
Noduration = (1-dutycycle)*Totduration; % duration of free time
% Time vector
t = linspace(0, Totduration, Totduration * samplingRate);
```

```
% Calculate frequency step
frequencyStep = (frequencyB - frequencyA) / (numFrequencies - 1);
% Initialize the waveform
wave = zeros(1, numel(t) * numFrequencies);
% Generate waves for each frequency
for i = 1:numFrequencies
    % Calculate current frequency
    currentFrequency = frequencyA + (i-1) * frequencyStep;
    % Generate the wave
    maxSamples = round(maxDuration * samplingRate);
        % No.of samples in maxduration
    nodursamples = round(Noduration * samplingRate);
        % Number of samples for the 0% duty cycle
    amplitude = [linspace(0, maxAmplitude, numel(t)/2-maxSamples/2-
        nodursamples/2), maxAmplitude*ones(1, maxSamples),
        linspace(maxAmplitude,0,numel(t)/2-maxSamples/2-
        nodursamples/2), maxAmplitude*zeros(1, nodursamples)];
    currentWave = amplitude .* sin(2*pi*currentFrequency*t);
    % Accumulate the waveforms
    wave((i-1)*numel(t)+1:i*numel(t)) = currentWave;
end
t1 = linspace(0,numFrequencies*Totduration,
    numFrequencies*Totduration*samplingRate);
% Plot the combined wave
plot(t1, wave)
xlabel('Time (s)')
ylabel('Amplitude')
title('frequency sweep signal')
```

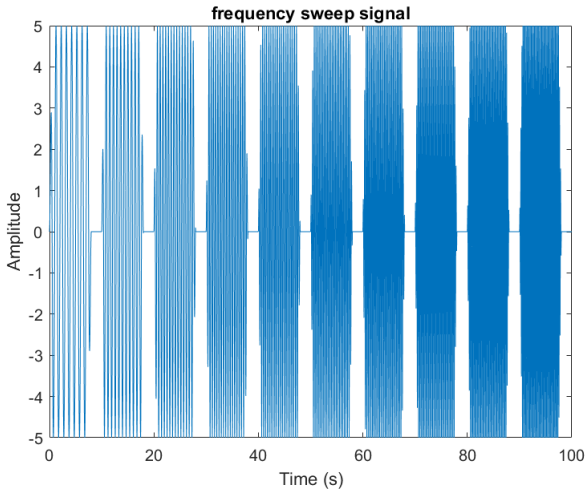


Figure 4.2: frequency sweep signal

## 4.2 C++ SDK

There are four distinct code files within the C++ SDK, each designed to serve specific functionalities. Let's delve into a detailed discussion of each of these files.

### 4.2.1 Simple Spectral Radar

This file comprises fundamental demonstration programs that illustrate how to utilize the SDK.

#### Simple Measurement

This code generates a simple B-scan pattern, allowing users to define the desired range and number of A-scans. Subsequently, it saves the processed data to a CSV file at the specified location.

#### Export Data and Image

This code generates a basic B-scan pattern, permitting users to define the desired range and number of A-scans. Additionally, it saves the processed data to both a CSV file and an image file at the specified location.

#### Averaging and Imaging Speed

To enhance image quality, this code offers two options. The first option is to reduce the scan speed, which increases the integration cycle time, resulting in improved image quality. The second option involves performing A and B-scans multiple times and calculating averages. This code executes these operations and generate a B-scan pattern and then saves the processed image at a user-specified location.

#### Volume Scan Pattern

This code creates a volumetric scan pattern, enabling users to specify the number of A-scans, B-scans, and the desired level of B-scan averaging.

#### Modify Scan Pattern

In a basic measurement setup, this code initially establishes horizontal scan patterns typically centered at (0.0, 0.0). It offers functions for rotation and zoom around the origin, followed by a shift of the origin point. Subsequently, a B-scan pattern is generated with these adjustments.

#### Continuous Measurement

This code offers functionality to contunously acquire multiple B-scans for the same defined B-scan pattern

### 4.2.2 Create Free Form Scan Patterns

This code serves as a demonstration of how to generate scan points using the Freeform Scan Pattern feature, which can be applied within ThorImage or integrated into other functions within the SDK. These scan points are formatted and saved in a standard TXT file, allowing for easy modification. The code enables the creation of scan pattern points for simple geometric shapes like circles, triangles, crosses, and more.

### 4.2.3 External Processing

This code offers a simple example of an external processing routine that reads raw OCT data from an input file, applies a basic processing step to each B-scan, and then writes the processed data to an output file. Its primary purpose is to showcase how external processing can be integrated with ThorImage to facilitate custom data manipulation.

### 4.2.4 Advanced Spectral Radar

#### Write OCT File

This program lets us to write data acquired with the SDK to an oct-file which can be viewed with ThorImageOCT. The generated oct-file is then stored in the same folder where the SDK is present.

#### Read OCT File

This program lets us read an oct-file with the SDK which has been acquired and saved with ThorImageOCT.

#### Write OCT File with free form scan pattern

In contrast to the previous Write OCT file function, this code allows for the utilization of custom, free-form scan patterns such as circles, triangles, or crosses, rather than being restricted to the standard straight-line pattern. Subsequently, the program generates an OCT file that can be easily read via ThorImage for further analysis and visualization.

### Processing Chain

The processing chain comprises multiple sequential steps, and using the SDK, it's feasible to access and work with the processed data at various intermediate stages, not just at the final step. This function empowers us to process the raw data acquired from the scan pattern using our customized processing routines. These routines encompass examples such as "Offset corrected spectrum," "Spectrum output," "DC corrected spectrum output," "Apodized spectrum output," and more.

### Advanced Modification of Scan Pattern

Using this code, it's possible to construct a scan pattern that consists of multiple consecutive B-scans acquired directly one after another. All B-scans within this pattern must have the same number of A-scans, enabling the creation of patterns involving rotating B-scans. One method to achieve such a pattern is to initially create a volume pattern and subsequently modify it using the functions 'shiftScanPatternEx' and 'rotateScanPatternEx'. These functions allow for the shifting and rotation of individual B-scans within the volume pattern. This code demonstrates the usage of the 'rotateScanPatternEx' function, while the use of 'shiftScanPatternEx' follows a similar approach.

### Free Form Scan Pattern

The freeform scan pattern functions provide users with the flexibility to generate 2D and 3D scan patterns of virtually any shape. These patterns can be defined using two distinct approaches. Firstly, users can specify only the edge points of the pattern, relying on interpolation methods to calculate the actual scan points within. Alternatively, users have the option to manually create all scan positions, which will be utilized exactly as provided without any interpolation.

### Removing Apo from Scan Pattern

In certain scenarios, it can be beneficial to eliminate the acquisition of additional apodization spectra during the processing routine to expedite the acquisition process. This can be achieved by conducting the acquisition of these apodization spectra before initiating the measurement, subsequently using them in the processing chain. By setting the number of apodization spectra to zero, no apodization is applied during the scan, resulting in faster scanning. Additionally, this reduces the time required for the scanner to reach the starting position of each scan, as only one flyback time is needed instead of two in the absence of apodization spectra acquisition.

### Doppler OCT

This code initially executes a standard processing routine to generate a B-scan pattern. Subsequently, it performs additional processing steps to perform Doppler OCT imaging. Users have the flexibility to define the output parameters for the Doppler processing and specify averaging parameters for the processing routine. Ultimately, the code carries out Doppler processing to obtain Doppler OCT images.

**Speckle Variance OCT**

This code begins by running a standard processing routine to create a volume scan pattern. It then proceeds to execute additional processing steps aimed at conducting Speckle Variance OCT imaging. Users are given the option to define averaging parameters for the processing routine as needed. Finally, the code calculates the speckle variance and exports the resulting data in CSV format to a user-specified location.

**External Trigger Modus**

This code offers the functionality to externally trigger the acquisition of A-scans. This capability allows users to synchronize measurements from various modalities, such as vibrometry and synchronized positioning, with an OCT measurement. It's crucial to ensure that the trigger signal initiates after the 'startMeasurement()' function and concludes after the 'stopMeasurement()' function. This demo program provides clear guidance on when to apply and disable the external trigger for proper synchronization.

### 4.2.5 Validation experiment

We acquired a simple B-scan pattern using ThorImage software and recreated the identical setup using the C++ SDK. Subsequently, we processed the data obtained through the SDK to generate images for a comparative analysis with those generated by ThorImage. The findings from this comparison are displayed below.

As depicted in Figure 4.4, we observe a B-scan with range of 2.19 mm and a depth of 3.56 mm. Within this range, 10,000 pixels correspond to 10,000 A-scans. To replicate a similar scan pattern as seen in ThorImage software, we provided the C++ SDK's "Modify Scan Pattern" function with these parameters, accounting for a noticeable origin shift present in ThorImage. The resulting scan pattern from the SDK was saved in a CSV file, a snapshot of which is displayed in Figure 4.5. By comparing Figure 4.4 and Figure 4.5, we observe that the depth information, in regions with multiple layers, appears to align between the ThorImage-generated data and that obtained through the SDK.


Figure 4.3: Validation Experimental Setup

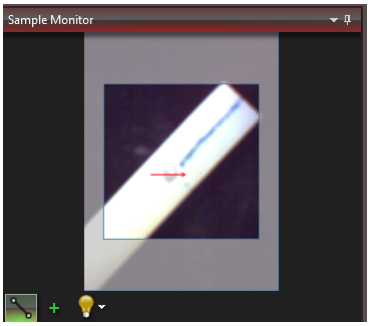


Figure 4.4: View of the sample for the experiment


Figure 4.5: Scan pattern specified in ThorImage software

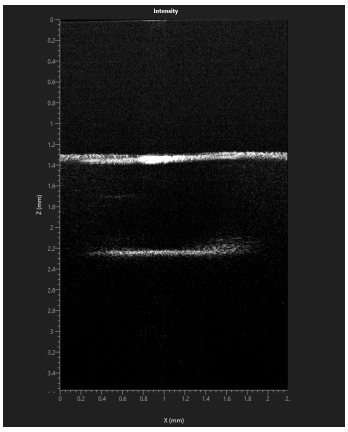


Figure 4.6: Obtained OCT image using ThorImage software

| | A | B | C | D | E | F | G | H | I | J | K | L |
|---|---|---|---|---|---|---|---|---|---|---|---|---|
| 1 | 18.2086 | 36.1738 | 37.3805 | 32.8234 | 37.4937 | 40.6337 | 33.8585 | 26.9528 | 36.8735 | 33.5327 | 41.8828 | 36.3484 |
| 2 | 33.9641 | 35.1246 | 41.6972 | 32.7152 | 22.8204 | 32.208 | 29.8755 | 33.4524 | 27.4284 | 26.3796 | 29.5035 | 32.4466 |
| 3 | 21.1591 | 27.1199 | 43.1181 | 33.3094 | 35.6302 | 29.9567 | 28.3932 | 34.4412 | 37.5956 | 30.7337 | 37.1182 | 26.9488 |
| 4 | 33.5093 | 33.8464 | 39.8499 | 24.8211 | 39.5357 | 35.1728 | 32.6548 | 31.5991 | 36.2472 | 33.1697 | 24.5816 | 28.1807 |
| 5 | 33.0181 | 36.7513 | 30.9602 | 43.7503 | 41.4524 | 32.8923 | 32.6793 | 31.6321 | 30.3872 | 39.3788 | 37.9065 | 31.7103 |
| 6 | 28.9511 | 28.0226 | 40.6841 | 34.2936 | 35.3531 | 29.1944 | 30.7391 | 29.0511 | 39.8 | 41.049 | 32.2444 | 29.0891 |
| 7 | 13.6586 | 35.995 | 41.364 | 35.8337 | 35.2438 | 43.0309 | 18.7498 | 42.9634 | 32.0352 | 34.0591 | 33.2798 | 37.1852 |
| 8 | 35.0926 | 43.371 | 42.8097 | 39.4017 | 38.0086 | 36.3862 | 37.7741 | 28.4366 | 38.5186 | 34.6521 | 34.2328 | 25.9776 |
| 9 | 39.7471 | 38.4311 | 42.5453 | 39.5022 | 36.8212 | 41.0435 | 35.5775 | 32.9541 | 37.1331 | 30.4181 | 31.4148 | 34.7094 |
| 10 | 36.5711 | 34.2188 | 44.8842 | 38.3527 | 40.6212 | 34.0368 | 31.4986 | 34.3609 | 34.7359 | 40.4945 | 35.9499 | 35.505 |
| 11 | 24.4724 | 29.0983 | 41.4967 | 35.0058 | 27.6226 | 11.1893 | 36.1324 | 31.383 | 31.2509 | 35.3314 | 35.3292 | 34.9208 |
| 12 | 33.6006 | 31.086 | 34.1115 | 24.0521 | 30.8524 | 24.7591 | 32.1115 | 27.1241 | 37.8123 | 27.2005 | 35.1086 | 37.0116 |
| 13 | 21.3423 | 36.5724 | 36.1613 | 39.2669 | 21.7709 | 42.1535 | 40.1299 | 29.682 | 32.5024 | 38.0383 | 41.6001 | 37.9303 |
| 14 | 32.2409 | 34.2144 | 33.1163 | 34.5867 | 31.219 | 29.9832 | 31.0727 | 23.3217 | 34.9195 | 22.7843 | 29.9472 | 27.4715 |
| 15 | 7.53896 | 40.6787 | 39.9829 | 39.0095 | 37.2989 | 36.2311 | 33.5871 | 26.8545 | 38.7636 | 27.6189 | 39.5461 | 34.2897 |
| 16 | -7.59768 | 36.3722 | 37.4245 | 42.1775 | 36.1856 | 33.763 | 37.0207 | 39.1264 | 28.7487 | 37.4548 | 24.8908 | 22.8225 |
| 17 | 30.9906 | 31.0869 | 32.5942 | 38.3821 | 36.8604 | 34.6557 | 11.4955 | 40.0799 | 34.4323 | 39.5972 | 39.4166 | 30.5443 |
| 18 | 35.3967 | 30.6544 | 42.7283 | 41.8373 | 41.6858 | 40.3316 | 39.6323 | 35.7468 | 34.5005 | 37.9325 | 38.2945 | 40.8124 |
| 19 | 22.6972 | 36.0911 | 31.9597 | 31.6572 | 38.2079 | 36.438 | 37.6076 | 35.8624 | 34.0894 | 32.335 | 29.3798 | 31.3201 |
| 20 | 29.2536 | 27.556 | 42.859 | 32.2799 | 42.7984 | 41.5064 | 37.5596 | 27.0309 | 39.2547 | 40.934 | 39.5703 | 26.6541 |
| 21 | 37.3862 | 27.0002 | 38.5644 | 41.0317 | 36.4933 | 40.6412 | 36.0521 | 32.3401 | 25.4469 | 31.9605 | 34.8794 | 35.266 |
| 22 | 19.9985 | 26.1804 | 39.8883 | 34.4603 | 38.8697 | 28.0961 | 33.625 | 29.4465 | 36.6283 | 39.4307 | 12.0934 | 36.0199 |
| 23 | 33.6757 | 21.1348 | 39.5834 | 36.6143 | 31.7989 | 41.1335 | 39.1723 | 29.9461 | 34.4527 | 27.3756 | 40.969 | 36.1018 |

Figure 4.7: Intensity data obained using SDK

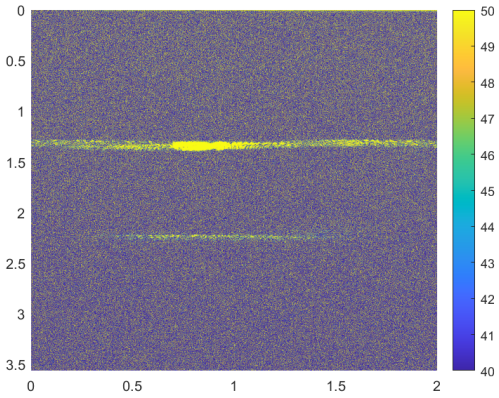


Figure 4.8: Post processed OCT image from data obtained using SDK

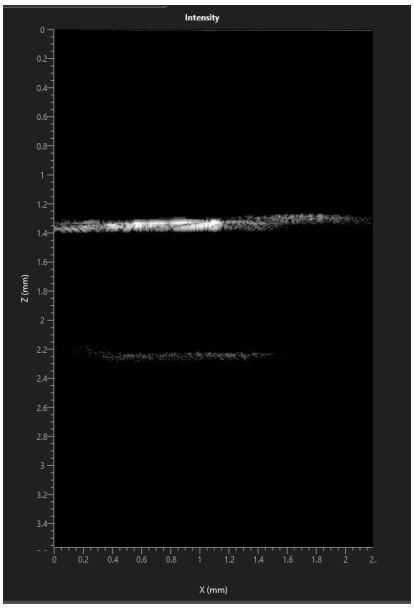


Figure 4.9: .oct file obtained using SDK opened in ThorImage

## 4.3 Handheld Otoscope

# Chapter 5

# Future Work

Currently, the SDK code is segmented into various modules, and the objective is to consolidate these modules, allowing for flexible combinations to create diverse code possibilities. This effort also involves identifying and documenting the necessary configuration file adjustments required when modifying or replacing individual components in the future. Ultimately, the overarching goal is to architect a robust and adaptable system, capable of accommodating changing requirements and evolving technological advancements, thereby enhancing the overall efficiency and versatility of the SDK.

We have received approval from the Institutional Ethics Committee (IEC) to conduct impedance experiments on human subjects. As a result, will be actively involved in both conducting the experiments and processing the data to obtain depth and vibrometry information.

To optimize our code, we aim to capture only the specific region of interest within the image, which will effectively reduce storage space requirements, acquisition time, and simplify post-processing of the data.

# References


[1] Nathan C. Lin. *Fiber-Optic Probe and Bulk-Optics Spectral Domain Optical Coherence Tomography Systems for in vivo Cochlear Mechanics Measurements*. PhD thesis, 2019. Copyright - Database copyright ProQuest LLC; ProQuest does not claim copyright in the individual underlying works; Last updated - 2023-03-03.

[2] Nathan C Lin, C Elliott Strimbu, Christine P Hendon, and Elizabeth S Olson. Adapting a commercial spectral domain optical coherence tomography system for time-locked displacement and physiological measurements. In *AIP Conference Proceedings*, volume 1965. AIP Publishing, 2018.

[3] Inc. ThorLabs. Telesto and ganymede series spectral-domain oct system base units user guide, July 2023.

[4] Inc. ThorLabs. Thorimage oct operating manual, May 2023.

[5] Peter H Tomlins and RK Wang. Theory, developments and applications of optical coherence tomography. *Journal of Physics D: Applied Physics*, 38(15):2519, 2005.

[6] Ruikang K Wang and Alfred L Nuttall. Phase-sensitive optical coherence tomography imaging of the tissue motion within the organ of corti at a subnanometer scale: a preliminary study. *Journal of biomedical optics*, 15(5):056005–056005, 2010.